Using a Novel Methodology to Constrain the Supermassive Black Hole-Galaxy Coevolution and Analyze the Selection Bias

Sahil Hegde, Shawn Zhang, Aldo Rodríguez-Puebla, Joel Primack

Abstract

In recent years, a major focus of astronomy has been the study of the effects of supermassive black holes (SMBH) on their host galaxies. Recent results have found strong correlations between SMBH mass and host galaxy properties, most notably in the bulge velocity dispersion and galaxy stellar mass. We utilize these relations along with a novel convolution method to construct number density models of different galaxy properties. Using these models, we compare two fundamental methods for constructing a black hole mass function (BHMF) with the $M_\bullet$-σ and $M_\bullet$-M_* relations. With these methods, we estimate the redshift evolution of the BHMF and, based on that, compare mass growth histories of central black holes and their host galaxies. Additionally, we utilize a data compilation of over 500 galaxies with individual measurements of galaxy properties (BH mass, stellar velocity dispersion, stellar mass, etc.) and classify galaxies by their morphologies in order to shed light on the controversial Shankar et al. (2016) argument that observations are biased in favor of massive SMBHs. We find that such a bias has little impact on the SMBH-galaxy relations. We conclude that the galaxy sample is a fair representation of the local universe and argue that our BH number density and scaling relations can be employed in the future to constrain relevant mechanisms for galaxy formation. We *emphasize* that this is the most comprehensive and accurate study of SMBH-galaxy coevolution as of now.

1 INTRODUCTION

The impact that active supermassive black holes (SMBHs) can have on their surrounding host galaxies is profound yet still poorly understood. In fact, the why, how, and when black holes alter the evolutionary pathways of their host galaxies remain as some of the major questions in astronomy.

One of the most important results has been the discovery that the masses of the central SMBHs are well correlated with the properties of their host galaxies, especially with the bulge properties (Magorrian et al. (1998); Gebhardt et al. (2000); Kormendy & Ho (2013)). This suggests that the formation of the galactic central black hole and the bulge are intimately correlated. While the relationship between the black hole mass and the bulge stellar velocity dispersion (σ) is often referred as the overall tightest relation, it is now well established that the mass of black holes also correlates with the total stellar mass of their host galaxy, although with larger dispersion (Reines & Volonteri (2015)).

It is generally accepted that the mass growth of SMBHs is largely through radiatively efficient gas accretion during the active quasi-stellar object (QSO) phase and as active galactic nuclei (AGN). Observations based on distant QSOs and AGNs show that the peak of the accretion rate density onto SMBHs was around $z \sim 2$, which was also the peak of star formation rate density (Merloni & Heinz (2008)). Moreover, there is ample evidence showing that the SMBH mass accretion rate and the star formation rate density are intimately correlated at least since $z \sim 3$ (Madau & Dickinson (2014)). This reinforces the idea that the relationship between SMBHs and their host galaxies is the key to understanding galaxy formation.

In this paper, we analyze over 500 distinct galaxies (a compilation of van den Bosch et. al (2016) and Reines and Volonteri (2015)) with individual measurements of black hole mass, stellar velocity dispersion, and stellar mass. We report SMBH mass-velocity dispersion and SMBH mass-stellar mass relationships and estimate the redshift evolution of the SMBH mass function derived based on these relationships. Finally, we present a simple model in which we measure the history of formation of black holes and galaxies.

1.1 Significance of Project

This paper's focus is to study the coevolution between galaxies and SMBHs over a broad range of the cosmic history of the Universe. Compared to previous studies that have derived the evolution of SMBHs based on empirical estimates from the stellar mass abundance of galaxies, we took the liberty of using the novel methodology of a convolution method as the basis of our research. This general method allows us to construct black hole masses not based solely on one galaxy property but to consider a large diversity of galaxy properties. In doing so, we establish a fair standard to see how the velocity dispersion and stellar mass methods compare in SMBH-galaxy coevolution, especially in evolution at high redshifts. This is actually the first time that a study has directly compared the two as a function of redshift and it potentially reveals a tighter agreement for the galaxy properties than previously noted.

In addition to comparing two different methods, we compared biased and unbiased relations and their results. Recently, Shankar et al. (2016) proposed that astronomical observations tended to detect higher mass SMBHs over lower mass ones. Hence, a bias in all such databases is prevalent and causes relations and results to skew towards the high mass end. This proposal has become very controversial, so we decided to investigate this possible bias. After confirming its validity, we used biased and unbiased datasets and formulated relations to directly compare the accuracy of our results. The fact that our coevolution was not significantly impacted from this bias makes us question how important this bias really is.

2 DEMOGRAPHICS FROM GALAXY CORRELATIONS

Imagine that we want to measure the number density function for galaxy property p for a complete sample of galaxies. Next, consider the galaxy property q and assume that the number density of this galaxy property is known as well as the relationship between p and q, i.e. $p = p(q)$, and the dispersion around it. Through this convolution, we can thus predict the number density of p from q using the following expression:

$$\phi_p\,(p) = \int_0^\infty P\,(p \mid q)\,\phi\,(q)\,dq \tag{1}$$

Provided $p = p(q)$ is known, it does not matter what p is, or how tight the correlation is between p and q; the number density can always be predicted very accurately from the above equation. For simplicity, we will assume that the probability distribution function of the galaxy property p is lognormal with mean given by the relationship $p = p(q)$ and dispersion given by the observed scatter in the relationship.

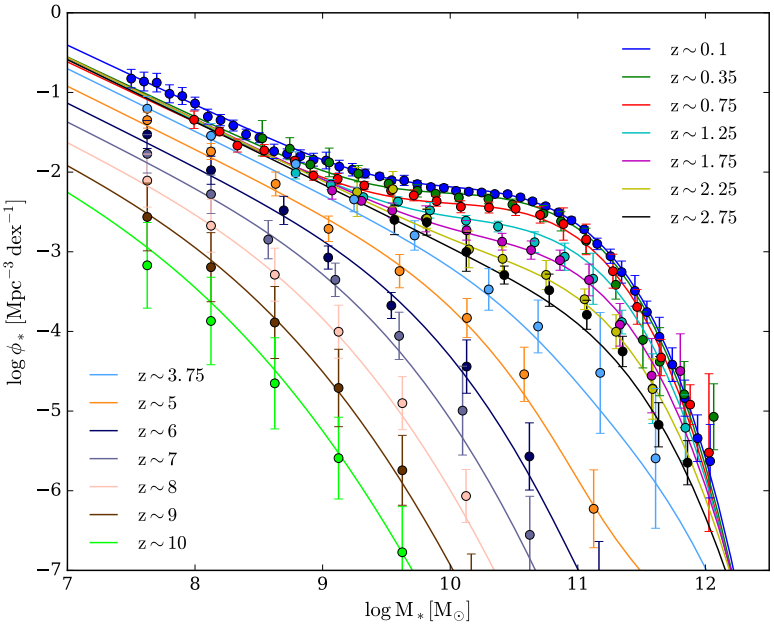

Figure 1: Galaxy Stellar Mass Function Redshift evolution from z ∼ 0.1 to z ∼ 10 of the galaxy stellar mass function (GSMF) derived by using a set of 22 observational samples represented with the filled circles with error bars. Solid lines are the best fit model from a set of 5×10^5 MCMC models.

One of the most fundamental properties of a galaxy is its stellar mass, M_*. Therefore, in this paper we will use M_* as a property q and its corresponding number density, known as the galaxy stellar mass function (GSMF) and denoted by $\phi_*(M_*)$, to derive the number density of a galaxy property p using Equation (1). Figure 1 shows the redshift evolution of the GSMF based on a compilation of 22 observational studies (Rodríguez-Puebla in prep.) from z ∼ 0.1 to z ∼ 10 (solid circles). The solid lines show the best fits to observations including several uncertainties affecting

the GSMF due to errors in individual galaxy stellar mass estimates, stellar population synthesis models, dust models, assumptions regarding star formation histories, and cosmic variance. This directly implies that when inferring the number density of a galaxy property p, we are effectively including observational errors in our modeling. This is important if our goal is to robustly understand how SMBH and galaxies regulate each other. We will also use the central velocity dispersion σ as another property q, and determine the Velocity Dispersion Function from observations.

In general, we will consider the following three observables: black hole mass $M_\bullet$, bulge stellar velocity dispersion σ, and stellar mass M_*. As mentioned earlier, the bulge stellar velocity dispersion is believed to be the tightest correlation between SMBH and galaxies. Here we will argue that the fact that observations show a correlation between SMBH mass and the total stellar mass suggests that the BH and the galaxy coevolve. Therefore, in our methodology we will consider two different methods in order to estimate the number density of black holes by using the $M_\bullet$-σ, $M_\bullet$-M_* and M_*-σ correlations. Below, we describe in detail our two methods.

3 REDSHIFT EVOLUTION OF THE $M_\bullet - \sigma$ RELATIONSHIP

In this section, we describe our methodology of inferring black hole number density from bulge stellar velocity dispersion. We begin by describing how using the M_*-σ correlation, we derive the σ number density, and then using the $M_\bullet$-σ relationship, we infer the black hole number density.

3.1 The $M_* - \sigma$ Relationship

It is now well established that in galaxies there is a fundamental relationship between the maximum circular velocity and total stellar mass. Broadly speaking, galaxies can be divided into two main classes: late-type galaxies (disk-like structures that are blue and star forming) and early-type galaxies with large red spheroids without significant star formation. The correlation between the maximum circular velocity and total stellar mass for disk galaxies is known as the Tully-Fisher relation (Tully et al. (1977)) while for spheroids it is known as the the Faber-Jackson relation (Faber et al. (1976)). While the Tully-Fisher relation refers to ordered motions of the stars in galaxies, V_c,

the Faber-Jackson relation represents disordered motions measured as the velocity dispersion of the stars, σ. However, simple arguments in virialized systems have shown that the relation $V_c = \sqrt{3}\,\sigma$ is accurate enough to convert the Tully-Fisher relation into a velocity dispersion relation (Binney & Tremaine (2008)). We will assume that the above relation is accurate enough at high redshifts. Note that this is a common practice for studying the dynamics of galaxies at low z (Dutton et al. (2011); Abramson et al. (2014); Rodriguez-Puebla et al. (2016)). Next, we show that the above assumptions are also consistent with observations at high redshifts.

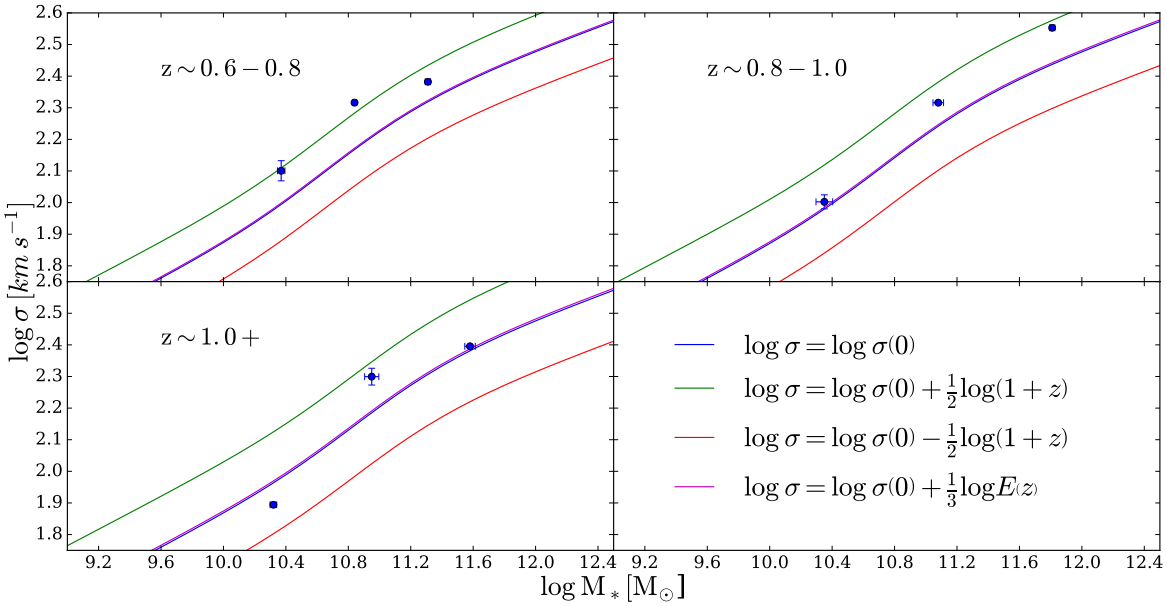

Figure 2: $\sigma - M_*$ General Relation Average velocity dispersion to stellar mass relation plotted at three redshift bins (blue line). We plot three experimental relations to test different methods of redshift evolution (blue, red, purple lines). We observe little difference between the average relation and the $E(z)$ relation because the expansion factor is insignificant at low redshifts.

Figure 2 shows the mean M_*-σ relation as the blue solid line, constructed by multiplying the Tully-Fisher and Faber-Jackson relations by the fraction of the universe populated by their morphologies. We compare with observations from di Serego Alighieri et al. (2005) at three redshift bins. We address the variation between the data values and the average curve by plotting three other hypothetical redshift evolutions as indicated by the labels in the plot. The relation which includes the expansion factor, $E(z)$ which represents the value of the Hubble parameter at different

epochs, was motivated by previous modeling based on large cosmological simulations (Rodriguez-Puebla et al. (2016)). Based on this plot, we conclude that the mean M_*-σ relation is consistent with little evolution in redshift, i.e. a possible time-independent correlation. We investigate this by comparing our resulting velocity dispersion function with more observational inferences at high z.

3.2 Velocity Dispersion Function

Based on the mean M_*-σ relation, we derive the velocity dispersion function (VDF) by using Equation (1). Figure 3 shows the resulting VDFs for five different redshift bins. Our results are indicated by the labels in the figure. We compare to observational determinations from Bernardi et al. (2010); Bezanson et al. (2012); Chae et al. (2011); and Abramson et al. (2014).

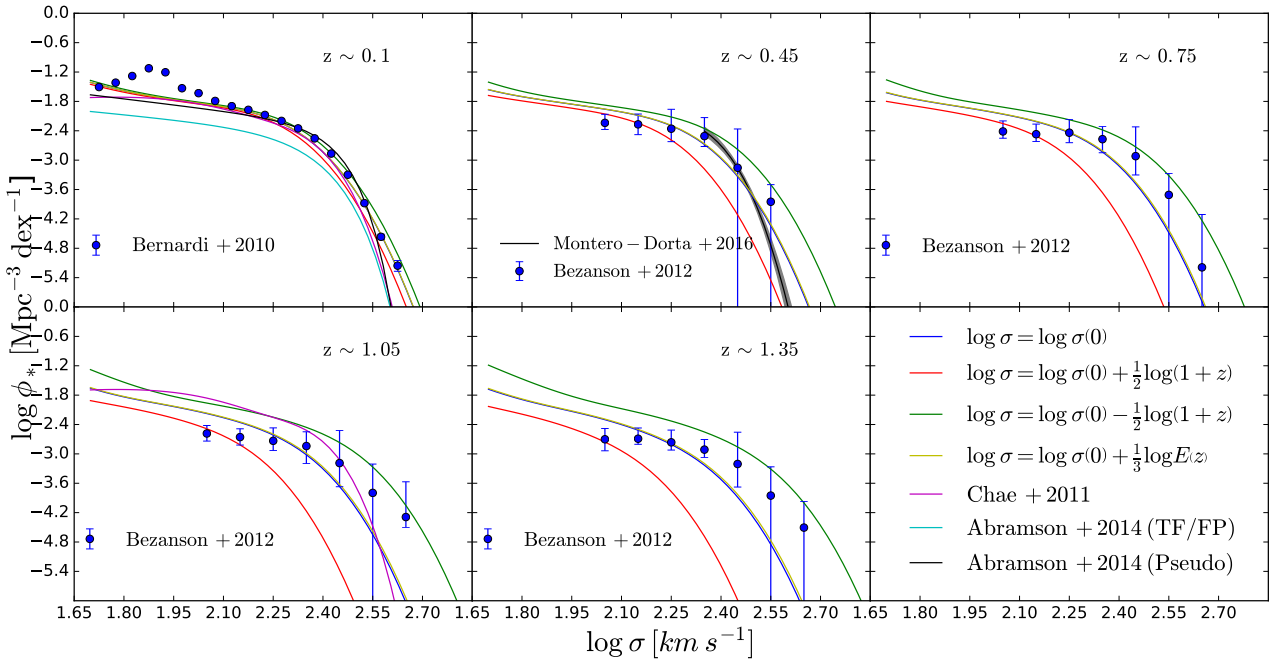

Figure 3: Velocity Dispersion Function Using Equation (1), we construct the number density function for bulge velocity dispersion (blue line) at five redshift bins. We once again test the three experimental relations (red, green, yellow lines) and compare our empirical model to observational determinations from Bernardi et al. (2010) and Bezanson et al. (2012) (solid blue points) and to those described in Chae et al. (2011) (purple lines), Abramson et al. (2014) (cyan and black lines), and Montero-Dorta et al. (2016) (black band). Once again, we observe that the expansion factor (yellow) is insignificant at lower redshifts.

We note that Abramson et al. (2014) reported two different VDFs indicated as TF/FP and Pseudo in the plot. The former is a similar method as employed in this paper while the latter is based on a more empirical general M_*-σ relation. We begin by noting that the relation given by a time independent M_*-σ relation is consistent with observations as well as the relation that evolved according to the expansion factor, $E(z)$.

3.3 The $M_\bullet - \sigma$ Relationship

Naturally, to construct the black hole mass function, we must determine the $M_\bullet$-σ relationship and the redshift dependence of this relation. Here we determine the $M_\bullet$-σ relationship based on a compilation of over 500 galaxies with individual measurements of black hole mass, stellar velocity dispersion, and stellar mass. Additionally, we use different published $M_\bullet$-σ relationships to derive an average relation and compare to our compiled data.

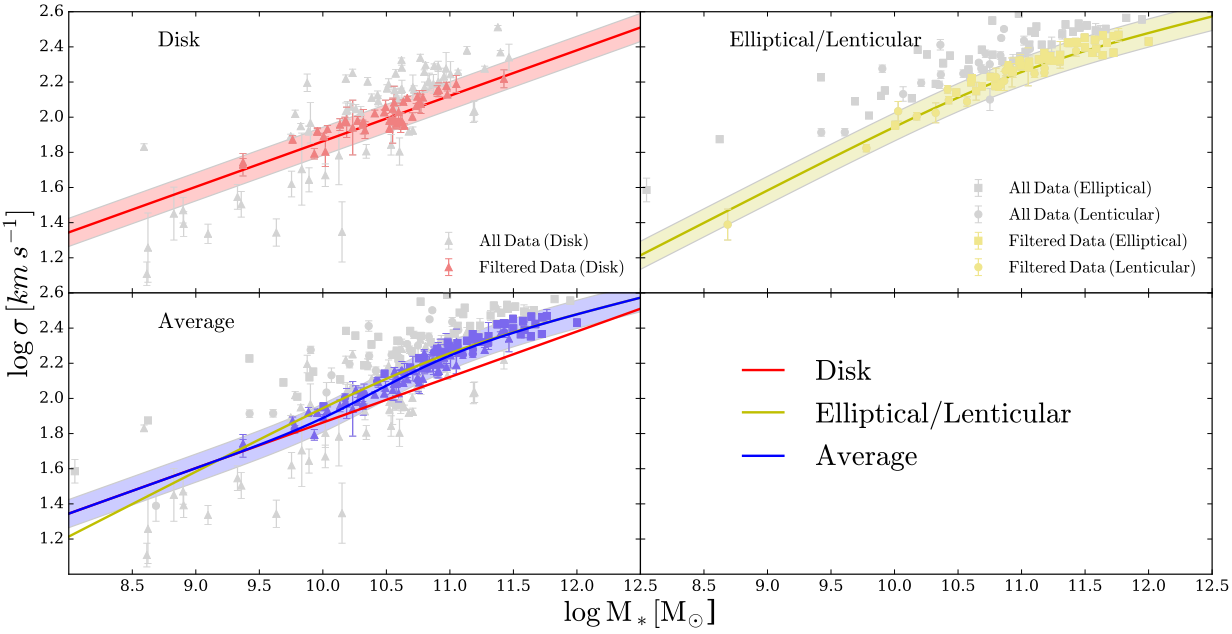

Figure 4: The Velocity Dispersion - Stellar Mass Relation: Tully-Fisher, Faber-Jackson, and Average Relations The three panels display the compilation of over 500 galaxies sorted into disk galaxies (Tully-Fisher, red band), elliptical galaxies (Faber-Jackson, yellow band) and the average σ-M_* relation (blue band). We filter the middle 68% of the data to evaluate effects of bias described in Shankar et al. (2016).

All the panels in Figure 4 show the M_*-σ relationship from our compilation (solid circles with error bars). The upper left panel shows this for galaxies with disk-like morphologies while the upper right panel of the same figure shows galaxies with spheroidal morphologies. We determined these morphologies based on a visual inspection of individual galaxies by using the SIMBAD Astronomical Database (http://simbad.u-strasbg.fr/simbad/). The first thing to notice is that not all our observed galaxies reside in the expected region based on the Tully-Fisher and Faber-Jackson relations. Note that the shaded areas indicate the region where 68% of the galaxies are expected to be found from observations. This difference is more dramatic for spheroids than for spirals. Since this could lead to a potential source of uncertainty in our results, we therefore decided to investigate this further.

We begin by noting that the above discrepancy has been reported in the previous analysis by Shankar et al. (2016) of the M_*-σ relation for galaxies with individual measurements of black hole mass. These authors argued that in order to achieve high accuracy in black hole masses, observations are usually biased to detect more massive black holes, resulting in systems that have large velocity dispersions and therefore empirically skewing $M_\bullet$-σ relationships above the true average. Here we test this hypothesis by selecting black holes that reside within the shaded areas and then studying if this skew biases the results observed in the $M_\bullet$-σ relation, which should be inherently independent of the skew of the dataset. Hereafter, we will refer to this as the filtered data.

The upper right panel of Figure 5 shows the $M_\bullet$-σ relationship of our filtered data and the entire data set. Note that our data does not occupy a different region compared to the unfiltered compilation. Moreover, we have quantified any deviations by fitting both the filtered data and all the data by using power-laws. Considering the best fit lines plotted for each type of relation in Figure 5, we see that there is little to no effect from filtering the data to fit the average relation for each type of galaxy. Thus, we conclude that the relationships derived can be safely used to construct the black hole mass function. The $M_\bullet$-σ relation we construct is of the following form:

$$\log \mathrm{M}_\bullet = 8.16 + 4.94 \log(\frac{\sigma}{200 \text{ km s}^{-1}}) \tag{2}$$

and the scatter around the relation is given by: $\epsilon_0 = 0.80$ dex.

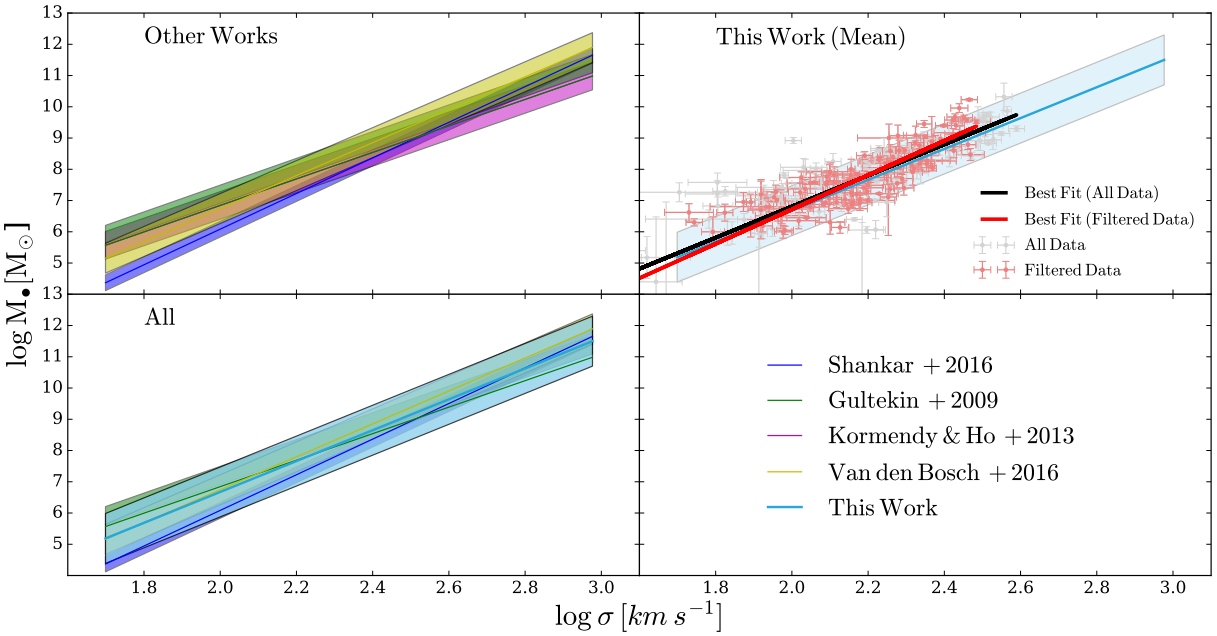

Figure 5: $M_\bullet - \sigma$ Relation We derive our $M_\bullet$-σ relation from four empirical models displayed with the scatter in Panel 1 (blue, green, magenta, yellow bands). Panels 2 and 3 display our derived relation as the light blue band with the scatter and compare it to the other models and the compilation data. Panel 2 also compares the filtered and unfiltered data from Section 3.4 and Figure 4 with the respective best fit lines for the two data sets.

3.4 High Redshift Relations of $M_\bullet - \sigma$

Before finalizing the relation as the derived black hole mass function, we experiment with different redshift evolution methods to evaluate the function at higher redshifts. Up to this point, the function has been constrained by data at low redshifts ($z \sim 0.1$ to $z \sim 1$). Thus, to create a mass function that is accurate at higher redshifts, we must test different methods of evolving it. We create the first method by evolving with the same factor as described in Larkin et al. (2016), which is similar to the one in Rodriguez-Puebla et al. (2016). Here, the expansion factor $E(z)$ is used and, as seen in Figure 6, the function shifts as a result. We also test the evolution using the black

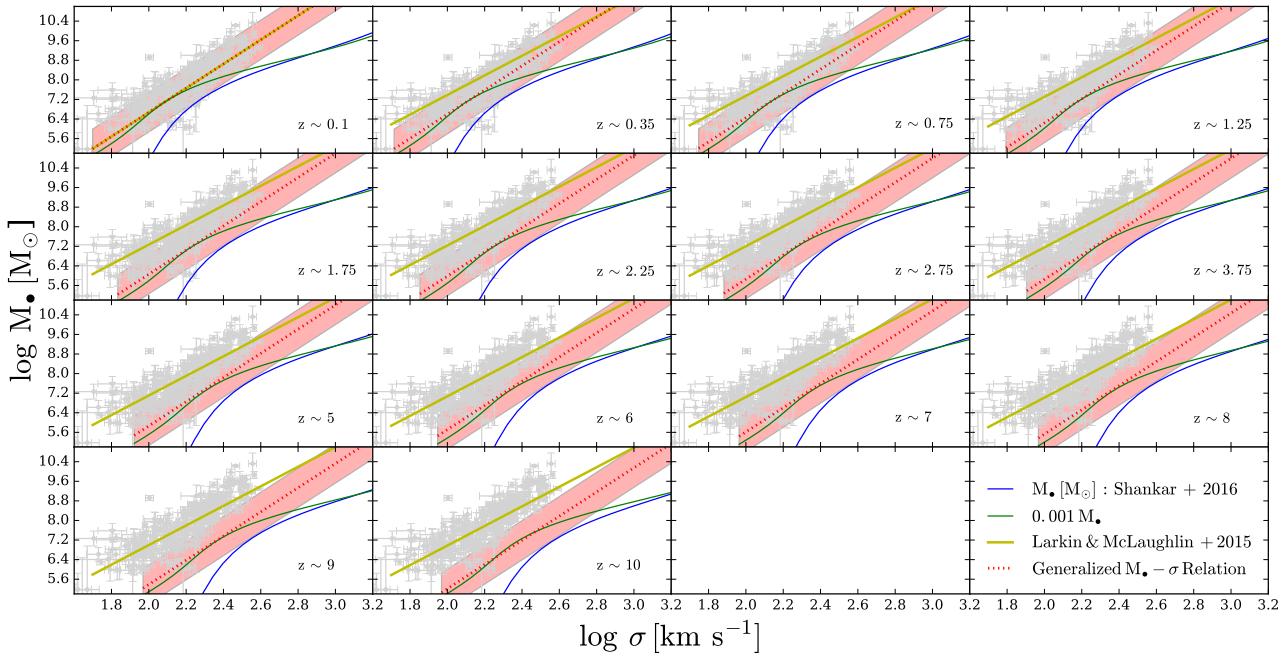

Figure 6: Different Redshift Evolutions The $M_\bullet$-σ relations plotted as the blue and green curves are combinations of Equations (3) and (4) with a circular velocity function. We manually calculate the shift of the two curves and apply that shifting factor to our generalized relation (red band) at each redshift panel. As a result, we observe the generalized relation shifting in conjunction with the blue and green curves.

hole mass function described in Section 5. We convert the two mass functions into $M_\bullet$-σ relations using the bisection method. Essentially what this means is given a velocity V_{max} density function and a black hole mass density function, we find common density values across the two functions and evaluate both to find the respective V_{max} and $M_\bullet$ values. Applying the same conversion factor as before ($V_c = \sqrt{3}\,\sigma$) allows us to approximate a $M_\bullet$-σ relation from a black hole mass function and yields the plot through which we can calculate the evolution. By manually reading the $M_\bullet$ and σ shifts from $z \sim 0.1$ to $z \sim 10$, we create the function shifts observed in Figure 7. As can be seen, the $M_\bullet$-σ relation evolves more drastically with the manually calculated shift, but both are fairly accurate calculations of high redshift relations.

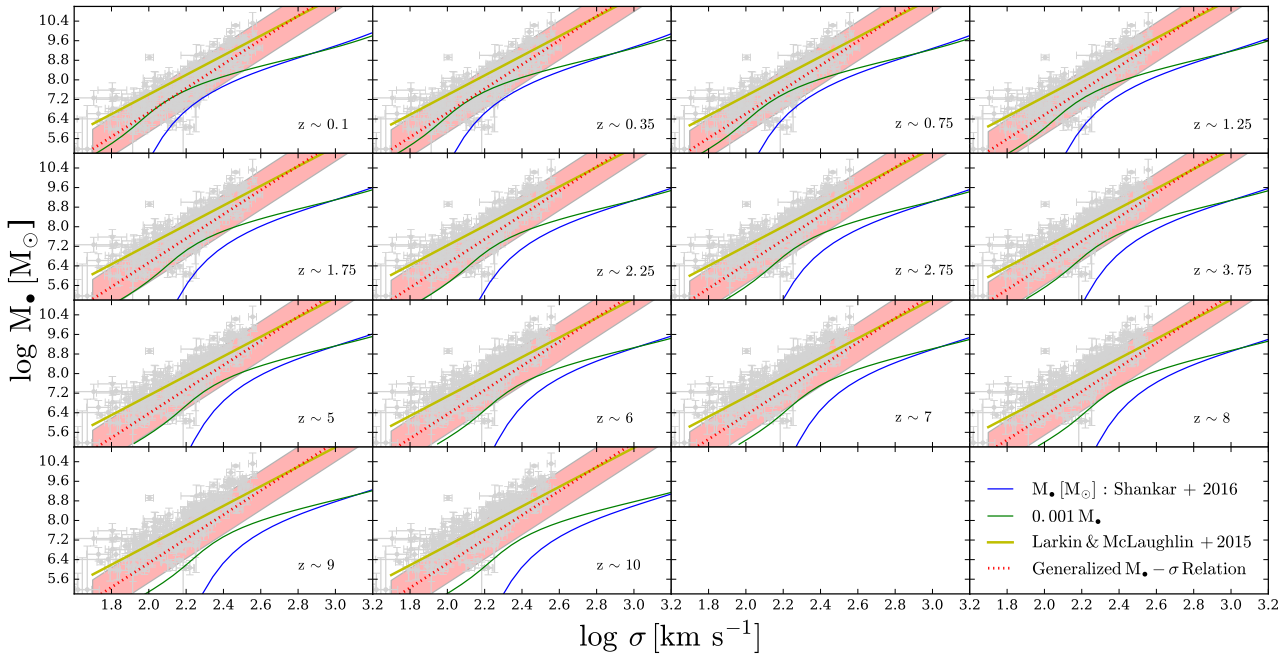

Figure 7: Evolution with Expansion Factor Here we plot a contrast to Figure 6 in using a different shifting factor to translate our generalized relation at higher redshifts. We apply the expansion factor from Larkin et al. (2015) (yellow line) and as a result, the generalized relation moves along with the Larkin relation.

4 THE $M_\bullet - M_*$ RELATIONSHIP

In this section, we describe the $M_\bullet - M_*$ correlations that we will use in order to create another method to estimate the number density of SMBHs.

As mentioned earlier, Shankar et al. (2016) argued that there is a potential bias in the way that galaxy samples with direct measurements of SMBH masses skew towards high masses. Based on their analysis, the authors claimed to have obtained the following intrinsic correlation for $M_\bullet - M_*$:

$$\log\left(\frac{M_\bullet}{M_\odot}\right) = 7.574 + 1.946x - 0.306x^2 - 0.011x^3 \tag{3}$$

where $x = \log M_* - 11$. In this paper, we will refer to this relation in our plots as $\mathrm{M}_\bullet[\mathrm{M}_\odot]$: Shankar + 2016.

The second relation we use is one obtained based upon direct black hole mass determination

from Marconi & Hunt (2003). This relation is supposedly "biased" and we will then use it to compare with Equation (3) and evaluate the bias's significance in our results. The equation has the form:

$$\log M_\bullet = \log M_* - 3.1 \tag{4}$$

where $M_\bullet$ and M_* are in solar masses. We will refer to it in our plots as $0.001\mathrm{M}_\bullet$.

Finally, we also calculate the $M_\bullet - M_*$ relation from the ~ 500 galaxies described in the previous sections. We fit the entire dataset through a linear regression and find the following relation:

$$\log\ M_\bullet = 1.28(\log M_*) - 6.25 \tag{5}$$

In order to test the bias argument, we used the filtered data described in Section 3.3 to obtain the following equation:

$$\log\ M_\bullet = 1.48(\log M_*) - 8.24 \tag{6}$$

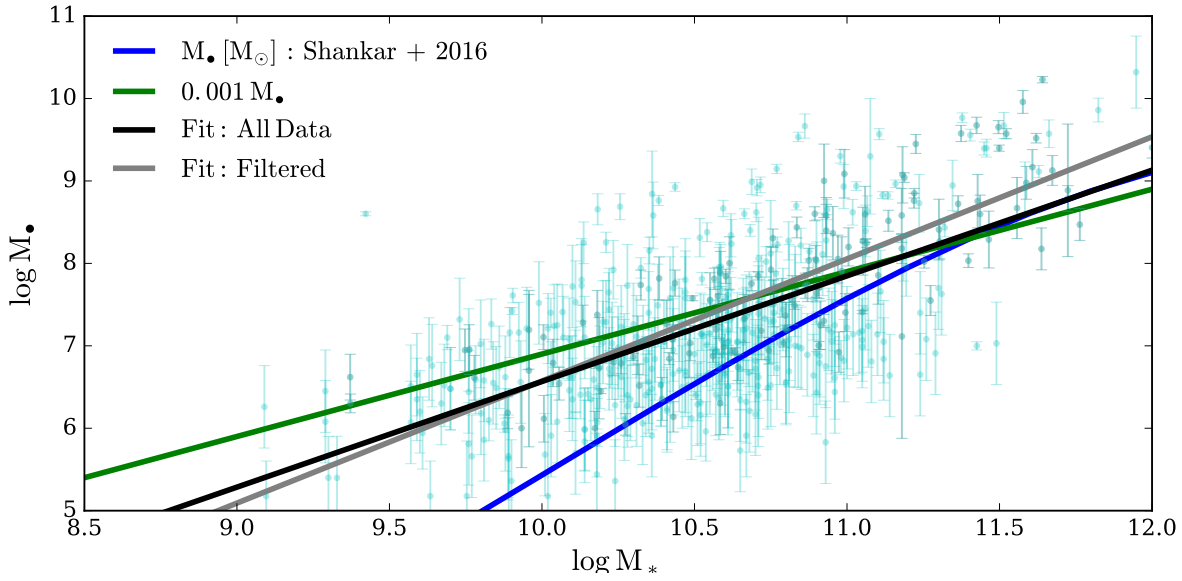

Figure 8: $M_\bullet - M_*$ Relation This figure plots the stellar mass of galaxies to the mass of their central SMBHs. We display all of the relations we stated above and compare them to the observational samples shown in the background.

Figure 8 shows the comparison between the relations and our SMBH sample. Notice that Equa-

tion (3) has a smaller curve as it tries to counter the bias. However, this bias could be exaggerated. To see this, we compare the filtered fit to the all, gray and black solid lines respectively. The filtered data actually does not reflect a strong bias. In fact, both linear regression relations are very similar and we conclude that our relations can be safely used to derive black hole mass functions (BHMFs). Finally, note that given the available range of stellar masses, we only consider SMBHs in the mass range $\log(M_\bullet/M_\odot) = 5$ to 11. Mass

5 DETERMINING SMBH NUMBER DENSITY

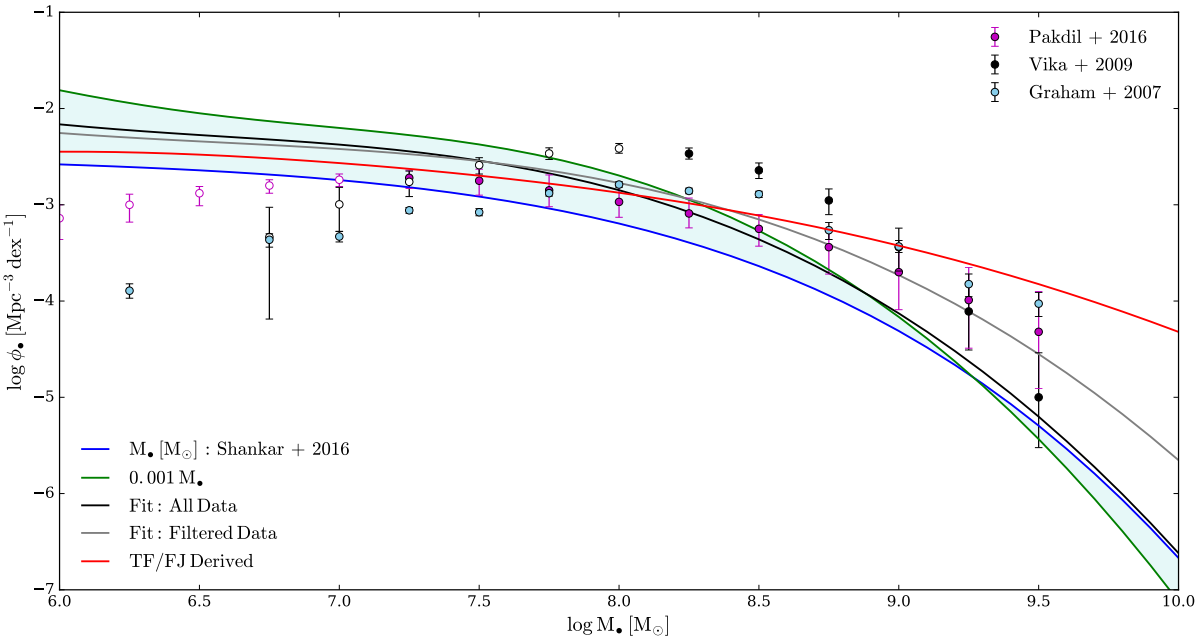

Figure 9: Mass Function at $z \sim 0$ We use Equation (3) as an upper bound and Equation (4) as a lower bound. This cyan band represents our uncertainty, as the true mass function lies somewhere within it. Observational samples from the literature show excellent correspondence with the functions for $M_\bullet > 10^{7.3} M_\odot$.

In this section, we describe our resulting SMBH mass functions by using the $M_\bullet - \sigma$ and $M_\bullet - M_*$ relationships obtained in Sections 3 and 4, respectively. In Section 2, we showed our robust methodology to find the number density of galaxies with a property p once the number density of a property q and their relationship $p = p(q)$ is known for those same galaxies. When

deriving our SMBH mass function, we assume that $p = M_\bullet$ and $q = \sigma$ or M_*. Note that when using $q = M_*$, $\phi(q)$ represents the GSMF while $q = \sigma$ is the VDF. See Section 2 for details.

Figure 9 shows the resulting SMBH mass functions at $z \sim 0$ from the $M_\bullet - M_*$ relations and from the $M_\bullet - \sigma$ relation described in Section 3. Despite the differences in deriving the relations, we observe that all the relations yield quite similar SMBH mass functions, especially from $M_\bullet < 10^{8.5} M_\odot$. On the same figure, we compare with observational inferences of the SMBH mass function from Pakdil et al. (2016), Vika et al. (2009), and Graham et al. (2007), and see relative agreement between our results and these past observations. More importantly, our resulting mass functions from the filtered data do not express systematic deviations from the previous relations.

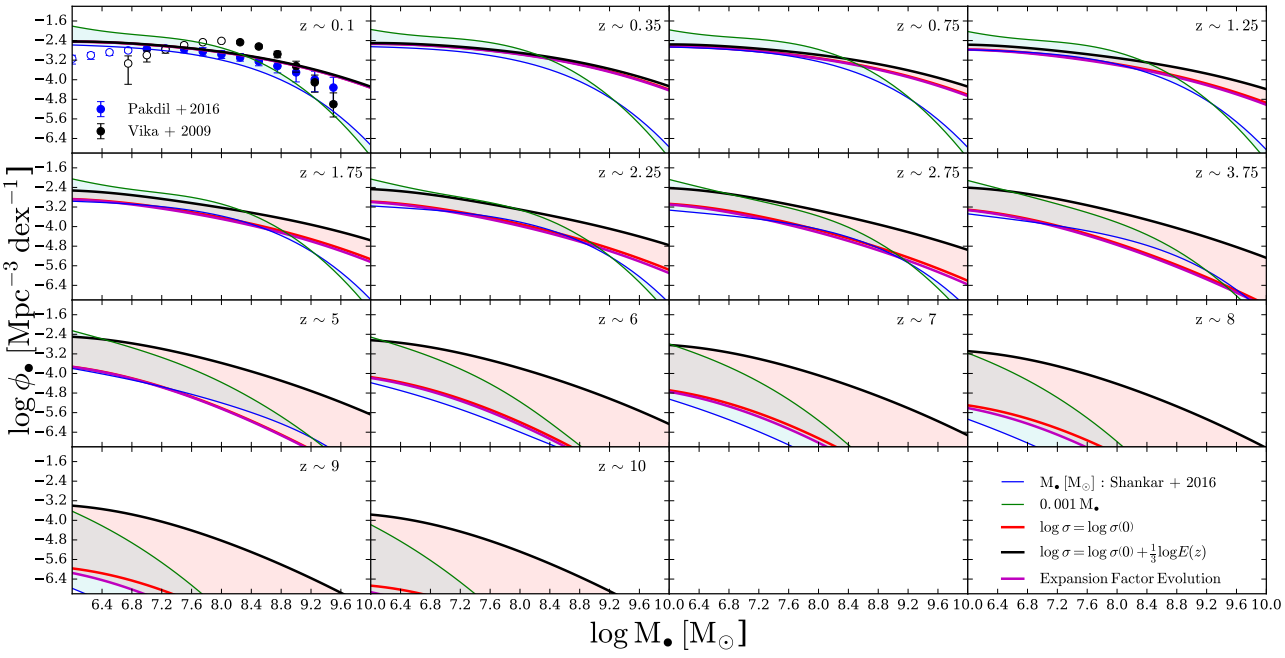

Figure 10: Black Hole Mass Function for $z \sim 0.1$ to $z \sim 10$ The figure displays the SMBH mass functions in redshift evolution based on our different derived methods. The velocity dispersion construction creates a band of uncertainty (pink) and is bounded by the expansion factor addition and evolution. The stellar mass construction is bounded by Equations (3) and (4) with a blue band.

Now, taking advantage of our method, we are also able to display the SMBH mass functions across higher redshifts. In Figure 10, we apply the shifts from Section 3.3 and compare the different methods of construction, examining their evolution. We find good agreement, indicating a stronger

correlation between velocity dispersion and stellar mass methods than previously believed. Note that there is a lack of observational data at these high redshifts. Additionally, since this is the first time that SMBH mass functions have been viewed at such extreme redshifts, it is difficult to compare with previous studies. Nonetheless, our BH number density and scaling relations can be used in future studies, constraining relevant mechanisms for understanding galaxy formation.

6 RESULTS

We will now report our generalization at high redshifts and derive the average growth of galaxies and SMBHs. Looking at how individual galaxies and SMBHs grow in mass, we can compare the shape and size of their plots to understand the results of this project.

6.1 Determining the average growth of galaxies and SMBHs

Here, we describe a model to determine the average stellar mass growth of galaxies and SMBHs. The basic idea relies on tracking galaxies at a fixed number density and then studying their progenitors and descendants as a function of cosmic time. In the absence of mergers, galaxies will grow in mass by in-situ star formation while their number density remains constant. Mergers do not conserve numbers, but if we ignore galaxy mergers, the mass growth of galaxies and SMBHs will result in a shift in the cumulative number density of the GSMF and SMBH mass function. More formally, we form and solve the following equation:

$$\int_{q_{t_p}}^{\infty} \phi(q, t_p) dq = \int_{q_{t_d}}^{\infty} \phi(q, t_d) dq \tag{7}$$

where q_{t_p} is the property of the progenitor at time t_o and q_{t_d} is the property of the descendant at time t_d. Note that $q = M_*$ for galaxies while $q = M_\bullet$ for SMBHs. Finally, we solve the above equation by fixing the number density at $z = 0$ and study the progenitors for galaxies with stellar masses $M_* = 10^9, 10^{9.5}, 10^{10}, ...10^{12} M_\odot$. We use the same number densities to track the progenitors for their corresponding SMBHs.

We begin by looking to Figure 11 and comparing the different black hole mass growth rates to evaluate the effectiveness of the relations we derived. In the top panel, the blue band represents the uncertainty in our predictions, bounded on top by the unbiased Equation (3) and below by the generally accepted but "biased" relation, Equation (4). Overlapping the band, we plot the filtered data fit and see strong agreement in shape and location on the plot, implying that our filtered fit is relatively accurate. The other two panels allow us to compare the shape and location of fluctuations in the fit from the entire data set (Panel 2) and the filtered data fit (Panel 3). Evidently, we can see little difference between each of the mass growth curves. This allows us to comfortably infer the resulting evolution of galaxies and SMBHs in Figure 12.

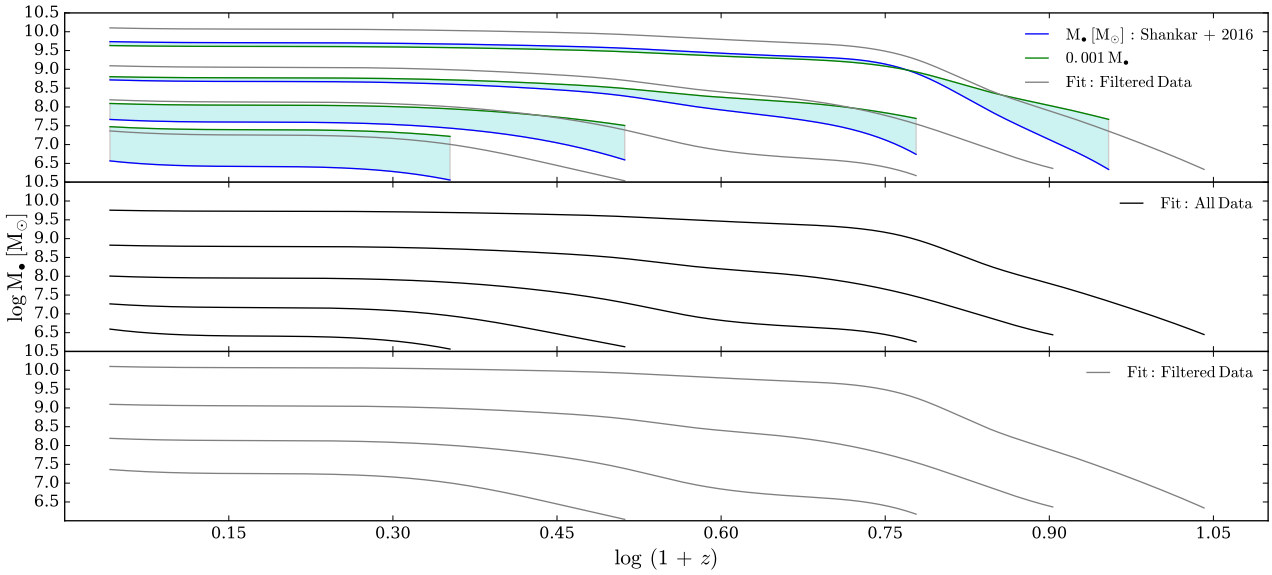

Figure 11: Black Hole Mass Growth The top panel contains a band with Equation (3) and Equation (4). We then plot the filtered data to evaluate agreement with the band. The bottom panels compare our unfiltered and filtered fits.

Figure 12 shows the comparison between galaxy stellar mass growth and black hole mass growth. Looking at the curves for each mass level, we see that the higher mass galaxies tend to gain mass rapidly in their early lives while the higher mass black holes do so concurrently. Also, when we look to the point of flattening for the two curves, we see that the galaxies and their corresponding black holes tend to stop gaining mass at approximately the same time in their lives (same redshift). We see this similar pattern represented in each of the other sets of curves between the

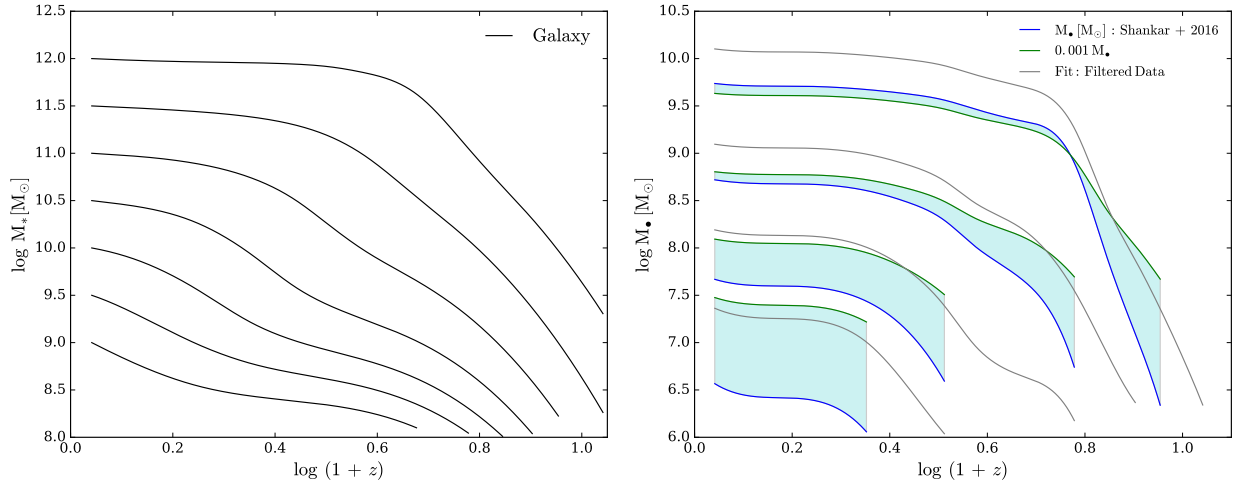

(a) Stellar Mass Growth **(b) Black Hole Mass Growth**

Figure 12: Mass Growth Comparison By comparing these two plots side by side, we see the rollover effect happen relatively at the same redshift. The left panel shows the progenitors of galaxies at $z \sim 0$ and the right panel shows their corresponding black holes at $z \sim 0$.

two plots, providing further evidence of a SMBH-galaxy coevolution.

7 DISCUSSION

The speculated reasoning for the causes of the coevolution of galaxies and their black holes follows the timeline of a galaxy's star formation rate. When a galaxy first forms in the early universe, it has rapid star formation as there are vast amounts of gas available. Massive stars explode as supernovae, ejecting dust and gas that is pulled back in and cycles back through the galaxy, to be reused to form more stars. We see this reflected in Figure 12 (a), as early on ($\log(1+z) \sim 1.1$ to 0.5), the galaxies of every mass bin have very high rates of growth. This is paralleled in the black hole mass growth plot as shown in (b), where the black hole rapidly gains mass for the early period of its life. The next portion of the evolution comes where the black hole reaches a peak mass and ejects all of the aforementioned dust and gas from the galaxy. Reaching that peak mass activates the SMBH and the galactic winds produced by the black hole prevent the dust and gas from reforming into stars. Additionally, our results confirm properties that we observe in galaxies today. The

higher mass curves on the plot generally represent the more massive, elliptical/spheroid galaxies that remain quiescent. We see this trend with mass reflected in the plots for lower mass galaxies, whose masses level off at lower redshifts (closer to current time). This same trend continues for the still lower mass spiral galaxies that are still actively forming stars today. Additionally, in terms of the black hole mass function, when looking to the results of the two relations for SMBH mass function construction ($M_\bullet$-σ and $M_\bullet$-M_*), we see strong agreement between the two functions, leading us to the conclusion that there is actually a stronger connection between the velocity dispersion and stellar mass than previously thought.

8 CONCLUSION AND FUTURE WORK

In our paper, we sought to study the coevolution between galaxies and SMBHs over a broad history of cosmic time. We exploit our novel convolution method to construct black hole mass functions based on a variety of galaxy properties. In this case, we specifically examined velocity dispersion and stellar mass methods. Not only did their respective SMBH mass functions show excellent agreement with past observational inferences, but they also showed agreement with each other. Note that throughout our study, we were worried about the effects of proposed bias by Shankar et al. (2016). By testing biased and unbiased relations, we discovered negligible differences between the two, making us confident in the validity of our results. Finally, by analyzing the rate of mass growth for individual galaxies and SMBHs, we notice agreement in shape and redshift and provide further evidence of a coevolution. Our black hole number density and scaling relations have incredible potential to be employed in future studies by constraining the relevant mechanisms for galaxy formation. With our method, comparison, tested bias, and evidence, we *emphasize* that this is the most comprehensive study yet of SMBH-galaxy coevolution.

In the future, we plan to analyze galaxies of different morphologies. In doing this, we would compare how the results differ based on spiral or elliptical classification. Additionally, we wish to investigate other galaxy properties besides velocity dispersion and stellar mass. We can then further directly assess agreement and correlation with our method. Finally, as we receive newer data, we

can explore the extent of bias in greater depths. By considering these additional factors, we become one step closer in understanding this phenomenon of SMBH and galaxy mass coevolution.

9 ACKNOWLEDGMENTS

This research could not have been conducted without the help of our mentor, Dr. Aldo Rodriguez-Puebla, and our faculty advisor, Prof. Joel Primack. We are incredibly grateful to them for the invaluable learning experience and the introduction to research. Additionally, we would like to thank the UCSC Science Internship Program for this tremendous opportunity. Altogether, this was definitely one of our most rewarding experiences thus far and we only hope that the program grows more and more in the future.

References

[1] Abramson L. E., Williams R. J., Benson A. J., et al., 2014, ApJ, 793, 14

[2] Bernardi M., Shankar F., Hyde J. B., et al., 2010, MNRAS, 404, 2087

[3] Bezanson R., van Dokkum, P., Franx M., 2012, ApJ, 760, 62

[4] Binney J., Tremaine S., 2008, Galactic Dynamics, 2nd edn. Princeton Univ. Press, Princeton, NJ

[5] Chae K. H., 2011, MNRAS, 413, 887

[6] di Serego Alighieri S., Vernet J., Cimatti A., 2005, A&A, 442, 125

[7] Dutton A. A., Conroy C., van den Bosch F. C., et al., 2011, MNRAS, 416, 322

[8] Faber S. M., Jackson R. E., 1976, ApJ, 204, 668

[9] Gebhardt K., Bender R, Bower G., et al., 2000, ApJ, 539L, 13

[10] Graham, A. W., Driver, S. P., Allen, P. D., et al., 2007, MNRAS, 378, 198

[11] Kormendy J. & Ho L. C., 2013, ARA&A 51, 511

[12] Larkin A. C., McLaughlin D. E., 2016, MNRAS, 462, 1864

[13] Madau P., Dickinson M., 2014, ARA&A, 52, 415

[14] Magorrian J., Tremaine S., Richstone D., et al., 1998, AJ, 115, 2285

[15] Marconi A., Hunt L., 2003, ApJ, 589L, 21

[16] Merloni A., Heinz S., 2008, MNRAS, 388, 1011

[17] Montero-Dorta A. D., Bolton A. S., Shu Y., 2016, ArXiv e-prints

[18] Pakdil B. M., Seigar M. S., Davis B. L., 2016, ArXiv e-prints

[19] Reines A. E., Volonteri M., 2015, ApJ, 813, 82

[20] Rodríguez-Puebla A., Behroozi P., Primack J., et al., 2016, 2016, MNRAS, 462, 893

[21] Shankar F., Bernardi M., Sheth R. K., et al., 2016, MNRAS, 460, 3119

[22] Tully R. B., Fisher J. R., 1977, A&A, 54, 661

[23] van den Bosch, R. C.E., Greene, J. E., Braatz, J. A., et al., 2016, ApJ, 819, 11V

[24] Vika, M., Driver, S. P., Graham, A. W., et al., 2009, MNRAS, 400, 1451